A Parallel Implementation of Semiclassical Transition State Theory

Chiara Aieta, Fabio Gabas, and Michele Ceotto*

Dipartimento di Chimica, Università degli Studi di Milano, via C. Golgi 19, 20133 Milano, Italy

E-mail: michele.ceotto@unimi.it

Abstract

This paper presents the parsctst code, an efficient parallel implementation of the Semiclassical Transition State Theory (SCTST) for reaction rate constant calculations. Parsctst is developed starting from a previously presented approach for the computation of the vibrational density of states of fully coupled anharmonic molecules (T. L. Nguyen et al. *Chem. Phys. Lett.* **2010**, 499, 915). The parallel implementation makes it practical to tackle reactions involving more than 100 fully coupled anharmonic vibrational degrees of freedom and also includes multidimensional tunneling effects. After describing the pseudo-code and demonstrating its computational efficiency, we apply the new code for estimating the rate constant of the proton transfer isomerization reaction of the 2,4,6-tri-tert-butylphenyl to 3,5-di-tert-butylneophyl. Comparison with both theoretical and experimental results is presented. Parsctst code is user-friendly and provides a significant computational time saving compared to serial calculations. We believe that parsctst can boost the application of SCTST as an alternative to the basic Transition State Theory for accurate kinetics modeling not only in combustion or atmospheric chemistry, but also in organic synthesis, where bigger reactive systems are encountered.

1 Introduction

Exact quantum expressions for the calculation of reaction rate constants have been available for many years now and computational methods for exact calculations are well established, ranging from state-to-state quantum reactive scattering to correlation function based methodologies.[1–9] However, the computational cost of quantum dynamical approaches scales often exponentially with the number of degrees of freedom (DOFs) of the system. Furthermore, they usually require a global knowledge of the potential energy surface (PES). An example of state of the art techniques is given by the family of Multi-Configurational Time-Dependent Hartree (MCTDH) methods, which achieve a convenient scaling with system size and are able to provide very accurate rate constants for full-dimensional processes involving a dozen of DOFs.[10–15] For kinetic modeling of complex chains of reactions, such as the ones involved in combustion and atmospheric chemistry, an estimate of the reaction rate constant for each elementary process in the kinetic model is requested. This leads to the necessity for many research areas to develop less sophisticated but still accurate methods for rate constant calculation.[16]

In general, Transition State Theory (TST),[17,18] and its modern implementations, such as Variational Transition State Theory (VTST),[19,20] provide a very useful approximation. Unlike dynamical methods, TST needs only few thermodynamic information about the reactive system. More specifically, only local knowledge of the PES in the surroundings of the saddle point and reactants wells are required. Unfortunately, TST has the intrinsic limitation of being a classical theory.

Even if the majority of chemical reactions are described adequately by classical mechanics, there are some cases, especially when a light atom transfer is involved, where a quantum mechanics treatment is mandatory to correctly reproduce experimental rates.[21] Development of approximate rate theories that recover quantum effects, such as tunneling of light particles or zero point energy contributions, are therefore important for a correct description of reactive processes. To address this task without performing the full dimensional quantum

dynamics calculations, a possibility would be to derive a quantum mechanical equivalent of the TST formula, since such an approach would be easier to implement than more rigorous dynamical approximations and could be more readily applied to complex reactions.

However, a rigorous quantum mechanical transition state theory (QTST) formulation is not straightforward. Many versions of quantum mechanical TST have been proposed. To cite a few examples, Ring Polymer Molecular Dynamics (RPMD) can provide QTST-like approximations,[22–24] and the same is true also for the Centroid Molecular Dynamics (CMD) method.[25,26] The Quantum Instanton (QI) theory[27–30] and Liao and Pollak's method[31,32] represent other examples of zero-time-limit quantum mechanical approaches to rate constant theory.

A central problem in formulating effective alternative QTSTs is represented by the need to avoid any further approximations in addition to the direct dynamics one, which is the classical-TST assumption that trajectories do not return to the reactant well once they have gone through the transition state. Typically undesired approximations are those that resort to the separation of a one-dimensional reactive TS coordinate from the remaining orthogonal degrees of freedom.

Semiclassical approximations of quantum mechanics do not require the separability of the degrees of freedom and they provide a fruitful framework to develop non separable quantum corrected rate approximations.[33] Historically, the semiclassical approach for unimolecular rate constants is represented by the Wentzel-Kramers-Brillouin theory (WKB).[34] This approach suggests that the probability of tunneling through a barrier depends exponentially on the imaginary action (a classical action computed on the upside down PES) accumulated between the two multidimensional trajectory turning points.[35] A theory that actually achieved the non separability of the reaction coordinate is the Semiclassical Instanton (SCI) theory,[36] that is also known in the physics community under the name of "ImF argument".[37–40] This approach is a short time approximation to the rigorous quantum mechanical definition of the rate constant in terms of the flux side correlation function[41] and uses the semiclassical ap-

proximation for the Boltzmann operator which involves classical trajectories evolution along the imaginary time axes. Unfortunately, to locate the semiclassical instanton trajectory could be quite cumbersome in high dimensional systems, therefore specific implementations of the theory have been presented to make it manageable for applications.[39,42–44]

A further development of SCI theory, that we think it is more amenable for practical applications, is represented by the Semiclassical Transition State Theory (SCTST) developed by Hernandez and Miller.[45] Starting from an expansion of the vibrational energy of the reactive system in terms of vibrational quantum numbers, the rate constant is provided in closed form from the normal mode frequencies and the anharmonicty matrix given by second order Vibrational Perturbation Theory (VPT2) at the transition state. There are several quantum chemistry codes, such as Gaussian16 and CFour, that routinely provide the needed information.[46,47] The SCTST special features are those of correctly including the direct dynamics transition state approximation and the non-separable coupling among all degrees of freedom, thus providing a non-empirical treatment of tunneling along a multidimensional reaction path.

Even if the complete PES is not necessary to compute SCTST rates, ab initio calculations to get barrier heights, vibrational frequencies and anharmonic couplings have to be very accurate to achieve quantitative agreement with experimental data.[48] Unfortunately, the evaluation of the anharmonicity matrix is prohibitive for many-atom systems at the level of post Hartree Fock methods. To alleviate this drawback, the Reaction Path Hamiltonian (RPH),[49] and the Richardson Extrapolation methods have been proposed to approximate the cubic and quartic derivatives used in non-separable semiclassical transition state theory.[50] Moreover, a reduced dimensionality version of QTST has recently been presented, which treats semiclassically only a relevant subset of the system DOFs.[51,52] Another issue with SCTST is that it is based on VPT2, which is not suitable to describe large amplitude motions. Therefore, an effective combination of SCTST technique with schemes for hindered internal rotation based on imaginary time propagation and fitting the exact energy levels as

a function of quantum numbers has been explored.[53]

We think that a convenient implementation of SCTST, that has already proven computational feasibility and chemical accuracy at the same time,[48] is provided along with the MultiWell program package, which is based on the application of the Wang-Landau Monte Carlo technique.[54–57] This approach was first employed to calculate fully coupled anharmonic vibrational density of states (DOS), and therefore partition functions, at equilibrium geometries.[58] Later, the same technique has been adapted in the sctst code of the suite for the calculation of generalized partition functions associated with the reaction transition state.[59] This approach achieves excellent agreement with experimental and (when available) exact calculations for many small size reactive systems.[48] More recently, our group has presented a parallelization strategy, which makes it possible to compute the vibrational DOS for minimum geometries up to more than 100 vibrational DOFs. This is the paradensum program, which is part of the MultiWell suite.[60]

In the present paper, we extend the parallel implementation to the sctst code of the MultiWell suite to make it possible to calculate rate constants for higher dimensional systems than done before with the SCTST approach. As a demonstration of the potentiality of the new algorithm, which we call "parsctst", we apply it to the rate constant calculation of the proton transfer isomerization reaction of the 2,4,6-tri-tert-butylphenyl to 3,5-di-tert-butylneophyl. This system consists of 135 vibrational DOFs treated in full dimensionality.

The paper starts by recalling the SCTST method in the next Section. Section 3 describes the parallelization strategy and how this has been implemented in the MultiWell suite of codes. Section 4 tests the accuracy of the parallel implementation. In Section 5 applications of the method are shown and Section 6 concludes with some perspective.

2 Summary of the Semiclassical Transition State Theory (SCTST)

Quantum reactive scattering theory gives the exact formulation for thermal rate constants in the gas phase as the following Boltzmann average

$$k\left(T\right)=\frac{1}{hQ_{r}\left(T\right)}\int_{-\infty}^{+\infty}dEe^{-\beta E}N\left(E\right) \tag{1}$$

where h is Planck's constant and Q_r(T) is the partition function for the reactants. The cumulative reaction probability (CRP) N(E) in Equation 1 is given by the exact quantum mechanical expression

$$N\left(E\right)=\sum_{J}\left(2J+1\right)\sum_{\alpha,\beta}\left|S_{\alpha,\beta}\left(E,J\right)\right|^{2} \tag{2}$$

which defines the CRP as sum of the probabilities to reach each attainable product state α starting from each initial state β available at a certain value of the total energy E and over all possible total angular momenta J of the system. In Equation 2, $S_{\alpha,\beta}$(E, J) are the scattering matrix elements. Their quantum mechanical computation is very demanding, especially for systems of high dimensionality, because it requires solving the Schrödinger equation (with scattering boundary conditions) for each value of the total energy E and angular momentum J.[1]

A more practical way to deal with the evaluation of the CRP, is given by the Semiclassical Instanton (SCI).[36,42] This approach approximates the CRP as a sum over periodic classical trajectories, each called an "instanton", on the inverted PES. In this framework the semiclassical CRP for a system with N degrees of freedom is

$$N\left(E\right)_{\mathrm{SCI}}=\sum_{k=1}^{\infty}\left(-1\right)^{k-1}e^{\frac{ikS(E)}{\hbar}}\prod_{j=1}^{N-1}\left\{2\sinh\left[\frac{ku_{j}\left(E\right)}{2}\right]\right\}^{-1} \tag{3}$$

where S(E) is the classical action of the trajectory and k is a positive integer. In Equation 3

$u_j(E)$ are the stability parameters and they are given by the eigenvalues $e^{\pm u_j}$ (with j=1,2,...,N-1) of the Monodromy matrix

$$M = \begin{pmatrix} \frac{\partial \boldsymbol{q_f}(\boldsymbol{q_0},\boldsymbol{p_0})}{\partial \boldsymbol{q_0}} & \frac{\partial \boldsymbol{q_f}(\boldsymbol{q_0},\boldsymbol{p_0})}{\partial \boldsymbol{p_0}} \\ \frac{\partial \boldsymbol{p_f}(\boldsymbol{q_0},\boldsymbol{p_0})}{\partial \boldsymbol{q_0}} & \frac{\partial \boldsymbol{p_f}(\boldsymbol{q_0},\boldsymbol{p_0})}{\partial \boldsymbol{p_0}} \end{pmatrix} \tag{4}$$

associated with the motion along the periodic trajectory, where $\mathbf{q_0}$ and $\mathbf{p_0}$ are the initial positions and momenta of the periodic trajectory, and $\mathbf{p}_f$ and $\mathbf{q}_f$ are their corresponding final values. The advantage of the SCI formulation for the CRP is that instead of solving the Schrödinger equation, classical trajectory simulations are run. Consequently, SCI scales roughly linearly with the number of degrees of freedom of the system. However, locating the instanton trajectory in the case of a high dimensional system has turned out to be a difficult task because of the coupling between the reactive and the bound nuclear modes.

In any case, the DOFs non separability cannot be neglected if corner cutting and multi-dimensional tunneling effects are to be treated correctly. In this regard, Miller showed that the same simple analytical form found in the separable case for the semiclassical CRP of Equation 3 is also valid in the general instance of a non-separable Hamiltonian if "good" action-angle variables I_n for the transition state are constructed.[61] More specifically, for bound modes, the Bohr Sommerfeld quantization rule is

$$I_n = \left(n_n + \frac{1}{2}\right)\hbar \quad \text{where} \quad n = 1, ...N-1,$$

while for the reactive mode, the quantization rule

$$I_N = \left(n_N + \frac{1}{2}\right)\hbar = \frac{i\theta}{\pi} \tag{5}$$

defines the generalized penetration integral θ. We introduce $\mathbf{n}\equiv(n_1,...,n_{N-1})$, the vector whose integer components are the quantum numbers that specify the state of each one of the N-1 normal modes vibrations with real-valued frequency of the transition state. Equation 5

allows one to write the energy as a function of the penetration integral θ, i.e. E($\mathbf{n}$, θ), since the Hamiltonian is written in terms of action-angle variables, i.e. $\hat{\mathrm{H}}$(I_1, ..., $\mathrm{I}_{\mathrm{N-1}}$, $\mathrm{I}_{\mathrm{N}}(\theta)$)=E. If one succeeds in inverting this relation to get θ($\mathbf{n}$, E), then the CRP is readily calculated

$$\begin{cases} N\left(E\right)_{\mathrm{SCTST}} = & \sum_{n_1=0}^{\infty}\sum_{n_2=0}^{\infty}\cdots\sum_{n_{N-1}=0}^{\infty}P_{\boldsymbol{n}}\left(E\right) \\ P_{\boldsymbol{n}}\left(E\right) = & \left\{1+\exp\left[2\theta\left(\boldsymbol{n},E\right)\right]\right\}^{-1} \end{cases} \tag{6}$$

The formulation of the SCTST by Hernandez and Miller consists in a strategy to provide this inversion in a simple way.[45,62] The starting point is the standard perturbative expression for the vibrational levels of a molecule with N vibrational degrees of freedom. For a configuration which corresponds to a minimum on the potential energy surface, if the total angular momentum is J = 0, the total vibrational energy can be expanded as

$$E\left(n_1,n_2...n_N\right) = V_0 + \sum_{j=1}^{N}\hbar\omega_j\left(n_j+\frac{1}{2}\right) + \sum_{j\leq j'=1}^{N}x_{jj'}\left(n_j+\frac{1}{2}\right)\left(n_{j'}+\frac{1}{2}\right) \tag{7}$$

where V_0 is the potential value at the bottom of the well, ω_{j} are the normal modes frequencies that are computed by diagonalizing the Hessian at the equilibrium geometry, and $\mathrm{x}_{\mathrm{jj'}}$ are the elements of the anharmonicity matrix that are computed from cubic and some of the quartic force constants. Equation 7 can be also generalized to the case of a molecular configuration that corresponds to a saddle point on the potential energy surface, i.e. a transition state. In this case, the N-th degree of freedom corresponds to the imaginary frequency and the following imaginary quantities can be defined as

$$\begin{aligned} \omega_N &= i\left|\omega_N\right| \\ x_{jN} &= -i\left|x_{jN}\right|, \;\; j=1,2...,N \end{aligned} \tag{8}$$

The expansion in Equation 7 is stopped at the second order, which is usually sufficient for the purpose of computing rates in the SCTST approximation.[63] By using Equation 5,

Equation 8 becomes a quadratic expression in θ. This form can be easily inverted to obtain the following generalized barrier penetration integral

$$\begin{aligned}
\theta\left(\boldsymbol{n}, E\right) =& \frac{\pi \Delta E}{\hbar \Omega_N} \frac{2}{1+\sqrt{1+\frac{4 x_{NN} \Delta E}{\left(\hbar \Omega_N\right)^2}}} \\
\Delta E =& V_0 - \left[E - \sum_{j=1}^{N-1} \hbar \omega_j \left(n_j + \frac{1}{2}\right) - \sum_{j \leq j'=1}^{N-1} x_{jj'} \left(n_j + \frac{1}{2}\right)\left(n_{j'} + \frac{1}{2}\right)\right] \\
\hbar \Omega_N =& \hbar \left|\omega_N\right| - \sum_{j=1}^{N-1} \left|x_{jN}\right| \left(n_j + \frac{1}{2}\right)
\end{aligned} \tag{9}$$

In the previous equations, V_0 is the potential at the saddle point, while the term in square brackets is the amount of energy that remains in the reactive mode characterized by the imaginary frequency.

3 Implementation

The evaluation of Equation 6 requires one to build all the vectors **n** of quantum numbers that give a total energy less than or equal to E and to evaluate $P_{\mathbf{n}}(E)$ for each of these states according to Equations 9. If the system consists of few degrees of freedom (up to 4 atoms) the direct count of the **n** states can be achieved via an iterative procedure.[64] However the number of combinations to be built increases very rapidly with the number of DOF of the system.

As already showed by Nguyen et al.,[59] a more convenient way to address this problem is to divide the energy range of interest into bins of width δE. In this way a certain number $\#_j$ of energy levels, each one identified by a **n** combination, will be found in the j-th bin, and the corresponding average reaction probability is defined as

$$\left\langle P\left(E_j\right)\right\rangle = \frac{\sum_{\boldsymbol{n}} P_{\boldsymbol{n}}\left(E_j\right)}{\#_j} \tag{10}$$

Therefore, the CRP can be rewritten as

$$N\left(E\right)=\sum_{j=1}^{E/\delta E}\delta E\rho^{\dagger}\left(E_{j}\right)\left\langle P\left(E_{j}\right)\right\rangle \tag{11}$$

where $\rho^{\dagger}$(E$_j$) is the vibrational density of states (DOS) associated to the real-valued frequency vibrations of the TS, and therefore δE$\rho^{\dagger}$(E$_j$) is the number of states in each energy bin. Within this approximation, the sum in Equation 6 over the accessible states is replaced by the easier sum over E/δE energy bins with energy lower or equal to the total energy E. As a result, the problem of evaluating the CRP is conveniently reduced to the computation of the vibrational density of states $\rho^{\dagger}$(E$_j$). Note that as δE is reduced, the result becomes more accurate.

We have already presented a parallel efficient computational approach that takes advantage of the MPI (Message Passing Interface) API (Application Programming Interface) for the calculation of the vibrational density of states.[60,65] That work was based on a previously published approach which relied on the Wang-Landau (WL) algorithm in the MultiWell program suite.[57–59] Here, we now adapt that parallel code to the computation of SCTST rate constants, and we name this new program parsctst. Its pseudo code is presented in Figure 1. In summary, the parallelization strategy to get the vibrational DOS is based on the division of the total energy range of interest into $\widetilde{\mathrm{W}}$ windows, where up to $\widetilde{w}$ random walks can run. Therefore, the code calculates on a single processor $\rho_{\mathrm{W,w}}$(E) with w=1,...$\widetilde{w}$, i.e. the DOS in each window energy range for each one of the walkers. Actually, for numerical convenience, the code handles $g_{\mathrm{W,w}}$(E)=ln[$\rho_{\mathrm{W,w}}$(E)]. Then, we include a certain percentage of overlap o between neighbor windows, which allows to join the quantities computed in different windows at the end of the computation to get total functions. The WL procedure starts with the selection of a valid starting vibrational configuration **n** for each independent walker. Next, a random walk over the vibrational configuration is performed. Every time a move is accepted the initial DOS guess is updated by the modification factor f along with

Algorithm 1 parsctst pseudo code.

Require: $\widetilde{\mathrm{W}}$, number of windows
Require: $\widetilde{\mathrm{w}}$, number of walkers
Require: o, overlap between neighbor windows
Require: fp, flatness percentage
Require: bal-key, window balancing keyword

Divide the whole energy range in $\widetilde{\mathrm{W}}$ windows with overlap o and balanced according to bal-key
Associate the W window to the W MPI process
for i=1, 21 **do**
  Initialize the histogram of visits $\mathrm{H_{W,w}(E)} = 0\ \forall$ W, w
  for w=1, $\widetilde{w}$ **do**
    if i=1 **then**
      Initialize: f = e, $\mathrm{g_{W,w}(E)} = 0\ \forall$ W, w
      Find an acceptable **n** in the window
    end if
    while min $H_{W,w}(E) > \overline{H_{W,w}(E)} \times fp$ **do**
      Select new **n** varying old one
      if **n** has an energy in the process window **then**
        Accept or reject the step
        $\mathrm{g_{W,w}(E)} = \mathrm{g_{W,w}(E)} + \ln(\mathrm{f})$
        $\mathrm{H_{W,w}(E)} = \mathrm{H_{W,w}(E)} + 1$
        if i=21 **then**
          Compute Ω_N associated to current **n**
          Compute ΔE associated to current **n**
        end if
      end if
    end while
    if i=21 **then**
      Average Ω_N and ΔE over the number of visits in each bin to obtain $\langle\Omega_N\rangle$ and $\langle\Delta E\rangle$
    end if
  end for
  Average $\mathrm{g_{W,w}(E)}$, over all walkers in the window
  Redistribute $\overline{\mathrm{g_{W,w}(E)}}$ to all w walkers in the window
  $\mathrm{f} = \sqrt{\mathrm{f}}$
  if i=21 **then**
    Average $\langle\Omega_N\rangle$ and $\langle\Delta E\rangle$ over all walkers in the window
  end if
end for
Normalize $\mathrm{g_{W,w}(E)}$ respect to the first non-zero element in the overlap
MPI reduction of $\mathrm{g_{W,w}(E)}$, $\mathrm{H_{W,w}(E)}$, $\langle\Omega_N\rangle$ and $\langle\Delta E\rangle$
Scale $\mathrm{g_{W,w}(E)}$ sequentially
Join $\mathrm{g_{W,w}(E)}$, $\langle\Omega_N\rangle$ and $\langle\Delta E\rangle$ from all with derivatives method
Compute the CRP

Figure 1: Pseudo-code of parsctst. The differences of the new parsctst implementation with respect to the paradensum algorithm[60] are highlighted in different colors. Blue stands for the general improvements to the WL parallel procedure which computes the DOS, while red indicates the extensions to the paradensum code to compute the CRP. W and w are the counter variables which span from 1 and respectively to $\widetilde{\mathrm{W}}$ and $\widetilde{\mathrm{w}}$ maximum values.

the histogram of visits $H_{n,w}(E)$ in the bin whose energy corresponds to the **n** configuration. When a walker satisfies the required flatness percentage *fp* for the histogram of visits, the modification factor f is decreased. At this point, in case of multiple walkers in the windows they average out their DOS estimate. Next, a new WL iteration starts with the estimate of the DOS from the previous one. In this way, the DOS function is more and more refined with each iteration. When a fixed number of iteration is completed, MPI reduction merges each processor data into a global array which includes the results of all windows. The width of the energy bins was set so that the lowest one in the first window contains just a single quantum state, i.e. the ZPE state. Therefore, the DOS values for the other bins are rescaled accordingly. The final DOS profile is built by joining the rescaled ones of different windows where $dg_{W,w}(E)/dE$ matches more accurately (derivatives method).

To obtain also the semiclassical CRP further operations are needed, as highlighted in red in the pseudo code in Figure 1. The average semiclassical tunneling probability $\langle P(E_i)\rangle$ of Equation 10 is actually obtained in the code by applying the procedure described by T. L. Nguyen et al.[59] During the last iteration, when a Monte Carlo move is accepted, Ω_N and ΔE of Equation 9 are computed with the current **n** quantum numbers. At the end of the iteration, the averages $\langle\Omega_N\rangle$ and $\langle\Delta E\rangle$ over the number of visits in each energy bin are obtained. After MPI reduction and matching of the chunks originated from each window, the $\langle P(E_i)\rangle$ is obtained by the evaluation of $\theta(\mathbf{n},E)$ and consequently $P_{\mathbf{n}}(E)$ according to Equations 6, where averaged values instead of the actual values of Ω_N and ΔE are considered. Finally, the CRP is computed using Equation 11.

3.1 Improvements to the Parallel Algorithm

To gain a better speedup in this version we include some new features, corresponding to the blue lines in the pseudo code of Figure 1. In the previous implementation (paradensum code) we noticed that the first window was usually slower in reaching the WL convergence than the others.[60] Sometimes for medium-sized molecules, however, we have observed that the last

window is the slowest. To alleviate this problem in this version we include the possibility to set windows of different width. In this way a slow window can be split in half so that the convergence is more quickly reached. The variable bal-key selects if the narrower windows are placed at the beginning or at the end of the energy range.

Another improvement respect to previous MultiWell implementations consists in the adoption of a faster strategy to start the random walks in each energy window. Before, a warm up random walk on the entire energy range was performed by each parallel process. In this way, the actual random walk, confined to the specific window, began when a starting point was found in that window.[60] This procedure makes the selection of initial vibrational state more favorable for regions with high density, usually the windows at higher energies. As a consequence, a misalignment of the threads appeared, because the random walks of windows with higher energy started earlier than the others. The new procedure is reported in Figure 2. It starts with the random selection of a vibrational quantum number which is increased by 1. Then, if the corresponding vibrational energy is not acceptable, because it is higher than the maximum energy in the window, or because the vibrational state would lead to molecular dissociation,[58] the modification of the quantum number is reset, otherwise it is retained. This procedure is iterated until a vibrational state with the energy in the process window is found. Tables 1 and 2 present the computational time saved respect to the basic implementation by employing these new features described above. Since the total computational time is given by the execution time of the slowest process (underlined in Tables 1 and 2), it is observed that a gain between 57% and 48% of the total execution time is attained with the same computational resources allocation. This means that the parallel architecture is much better exploited than before. This is confirmed also by speedup results discussed in the next section.

Algorithm 2 Selection of random walks starting point.

Require: E_{min}, minimum energy in the window
Require: E_{max}, maximum energy in the window

1: Initialize: $\mathbf{n} = 0$
2: Randomly extract a vibrational quantum number n_i
3: $n_i = n_i + 1$
4: **if** Dissociation check of **n** is not passed **then**
5: $n_i = n_i - 1$
6: **else if** $E_{min} < E < E_{max}$ **then**
7: END
8: **else if** $E < E_{min}$ **then**
9: Go to statement 2
10: **else**
11: $n_i = n_i - 1$
12: Go to statement 2
13: **end if**

Figure 2: New random walk starting point selection procedure. **n** is the vector of the vibrational quantum numbers n_i. The "dissociation check" procedure is described in reference[58].

Table 1: Time gain due to imbalanced windows in the CRP calculation of the Aryl radical 2-4-6-tri-tert-butylphenyl. The simulation has been done with 4 windows and with fp=50% flatness criterion. The execution time of each W parallel process is reported. The total execution time is dictated by the slower rank and it is underlined. Column "Time old" refers to the old implementation scheme, and "Time new" is the execution time obtained with the imbalanced windows.

W	Time old (s)	Time new (s)
4	960	1440
3	1020	1860
2	1440	840
1	<u>4200</u>	<u>1800</u>

Table 2: Time gain due to imbalanced windows and new starting point selection procedure of Figure 2 in the CRP calculation of the Aryl TS. The simulation has been done with 8 windows and with fp=50% flatness criterion. The execution time of each W parallel process is reported. The total execution time is dictated by the slower rank and it is underlined. Column "Time old" refers to the old implementation scheme, "Time new" is the execution time obtained with the imbalanced windows and "Time new start" adds the contribution of the new starting point selection procedure.

W	Time old (s)	Time new (s)	Time new start (s)
8	420	540	516
7	480	660	543
6	540	660	621
5	540	780	711
4	600	960	798
3	780	<u>1260</u>	<u>1182</u>
2	1140	600	534
1	<u>2280</u>	1030	1014

3.2 Scalability

In this section we analyze the parallel performance of parsctst code. We take into account two systems. The transition state (TS) of the Cl + CH_4 reaction, a system of small dimensionality, and the high dimensionality example of the transition state of the reaction of the 2,4,6-tri-tert-butylphenyil to 3,5-di-tert-butylneophyl (Aryl TS) with 135 vibrational DOFs. All simulations were done with a single walker per window and with 95% flatness criterion (fp). The speed up and the parallel efficiency are displayed in Figure 3. We define the speed up as the ratio of the execution time with a certain number of parallel processes equal to the number of energy windows, to the serial execution time with a single energy window. Instead, the parallel efficiency measures how well the computational resources are exploited by parallel execution. It is defined as the ratio of the speed up to the number of cores employed. In the case of the TS of the Cl + CH_4 reaction, the efficiency is always above the 60% and the performance gets worse by using more and more parallel processes. This happens because

this system is small. We also observe that the best performance in this case is achieved with equally balanced windows, for which a superscalability behavior is found if two or four cores are employed. This phenomenon occurs because executing the code with a single MPI process and running it with more MPI processes implies also that a different algorithm is exploited in the two cases. Specifically, when parsctst is run serially there is just one energy window, while many windows are set when the code is run in parallel. Therefore, the parallel code does not only take advantage of more computational resources than the serial one, but also it uses a more efficient algorithm, which can lead to the observation of superscalability when the chosen windowing scheme is particularly suitable for simulating a certain system. However, the parallelization was designed for systems of higher dimensionality and when the Aryl TS is simulated, the parallel performance of the code is almost ideal, i.e. always above the 90% for all test cases we considered. This result is obtained also thanks to the uneven set up of the energy windows, which are set narrower at the beginning of the energy range.

3.3 Influence of Flatness Criterion and Multiple Walkers

In the previous paper we investigated the possible computational impact of running multiple walkers on the code performance.[60] In that case, we compared simulations for the vibrational Density of States (DOS) calculations using one walker per window at 95% of flatness (*fp*) with the averaged DOS obtained from 10 or 100 separate simulations with still a single walker in each energy window but at a lower 80% *fp*. Our conclusion was that a straightforward parallelization of the code at walker level was not convenient since one had a worse accuracy than doing a single run with higher flatness. However, in the code the multiple walkers are implemented in such a way that they average out their DOS estimate at the end of each Wang-Landau iteration. This intermediate averaging turns out to have a significant impact on the code performance.

To prove this, for different flatness criteria, we have compared the computational effort and the accuracy of the DOS calculations performed with a single random walk in each

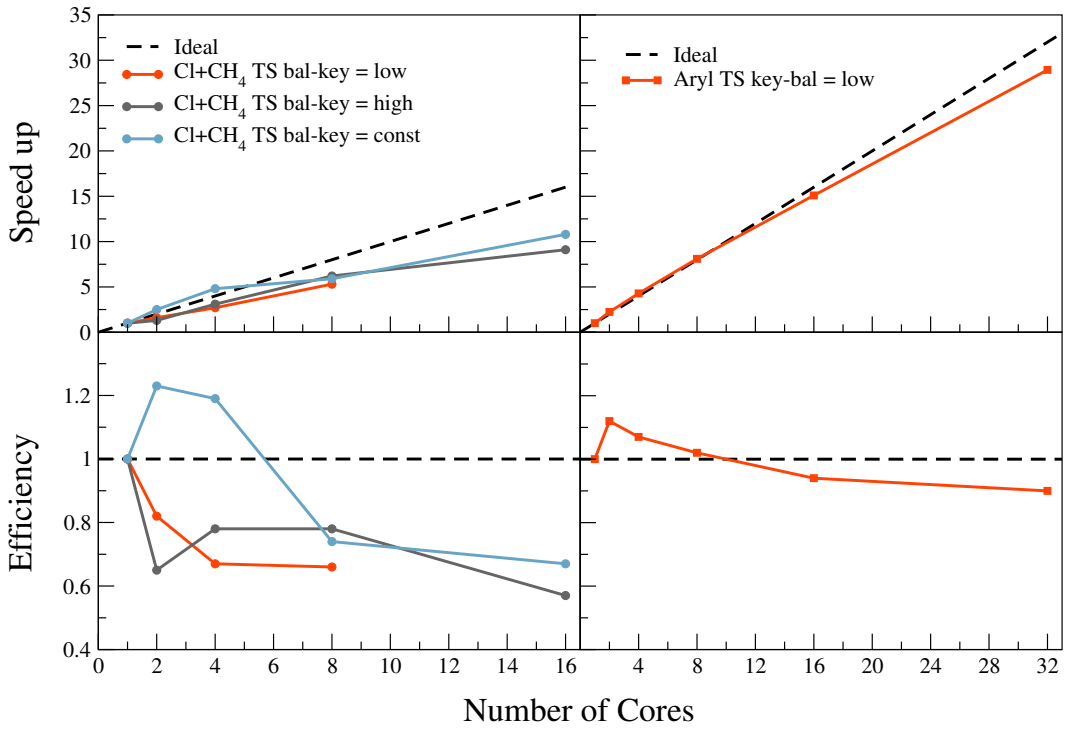

Figure 3: The upper panels report the speed up of parsctst code when the TS of the Cl + CH_4 reaction (left) and the transition state of the reaction of the 2,4,6-tri-tert-butylphenyl to 3,5-di-tert-butylneophyl (Aryl TS) (right) are simulated. The lower panels illustrate the corresponding parallel efficiency. The "const" value of the bal-key parameter means that the energy windows are evenly distributed along the total energy range. Instead, "low" indicates that smaller windows are set at the beginning of the energy range, while "high" means that smaller windows are set at the end of the energy range.

window with the computations done with multiple walkers in the same window. We choose to test two cases as significant benchmarks, i.e. the water molecule and the TS of Cl + CH_4 reaction. We used the paradensum updated with the improvements described above in Section 3.1 for the water molecule and the parsctst code for the TS of Cl + CH_4 reaction. For both systems we fixed the number of energy windows and computed the DOS with an increasing number of walkers per window and the simulations were repeated 10 times with different Monte Carlo seeds. For each simulation, every walker was initialized with a different seed for the generation of the random number chains. In this way the random walks are completely independent. We computed the Mean Relative Error (MRE) of the DOS simulations using the formula (12)

$$MRE_j = \frac{1}{N_{bins}} \sum_{i=1}^{N_{bins}} \frac{|DOS_i - Ref_i|}{Ref_i} \times 100 \qquad j = 1, \ldots, 10 \tag{12}$$

where N_{bins} is the total number of energy bins in the whole energy range. The energy bins are labeled by the i index. DOS_i and Ref_i are respectively the values of the computed DOS and the value of the DOS taken as a reference at the energy of the i-th energy bin. The j index labels the simulations of the global DOS function. To obtain the reference values (Ref_i) we used the MultiWell program suite doloop code for the water molecule.[58] Given the 3 vibrational degrees of freedom of water, the exact evaluation of the DOS is doable and it is considered as the reference for DOS accuracy. Differently, for the TS of Cl + CH_4 reaction DoLoop calculation of the DOS is not feasible. In this case we took as a reference the DOS calculated with a single simulation at 99% *fp* and using 100 walkers for each energy window. Then, we evaluated the average MRE ($\overline{\text{MRE}}$) and the corresponding standard deviation value σ, which are the measure of the accuracy of the results. In addition, to evaluate the computational effort, we calculated the average Steps To Flatness (ave-STF), which is obtained by averaging the total number of Monte Carlo steps needed to reach the convergence over all possible j independent runs.

Panel (a) in both Tables 3 and 4 shows the results from a set of simulations done with

a single walker in each energy window and by increasing the flatness criterion. The $\overline{\text{MRE}}$ and the standard deviation σ values become smaller when the flatness value *fp* is increased. This trend suggests that if it was possible to do a simulation with a 100% *fp*, the $\overline{\text{MRE}}$ and σ would be equal to 0. However, this simulation is impossible in practice, because it would require an excessive computational effort. Panels (b), (c), (d), (e) and (f) of Table 3 and panels (b), (c), (d) of Table 4 show how $\overline{\text{MRE}}$ and σ converge to a given value as the number of walkers is increased at a fixed flatness criterion. It is important to point out that if the *fp* is too low, the density of states cannot be improved indefinitely by increasing the number of walkers in each energy window. In fact, as clearly shown in panel (b) of Table 3, the $\overline{\text{MRE}}$ reaches a plateau when the number of walkers is raised from 10^3 to 10^4, while the values of σ reduces.

We turn now to the computational effort evaluation. By comparing the ave-STF and the $\overline{\text{MRE}}$ of the 99.9% *fp* calculation (panel (a) of Table 3) with the 100 walker simulation (panel (d) in the same Table) we conclude that multiple walker simulation at a sufficiently high flatness criterion can reach an accuracy comparable with a single walker simulation but at higher flatness. The same conclusion can be reached by comparing the 99.9% *fp* calculation reported in the panel (a) of Table 4 with the 100 walker simulation of panel (b) of the same Table. A closer look at these results shows that choosing lower *fp* and by increasing the number of walkers brings more precise and accurate results at a lower computational effort. For instance, in Table 3, the same or even better accuracy and precision than the single-walker simulation with 99.99% *fp* in panel (a) is achieved by simulations with 90% (panel (d)), 95% (panel (e)) or 99% (panel (f)) using multiple walkers for a total of less MC steps. The same observation can be deduced from the data reported in Table 4. Here, for example, a single-walker simulation at 99.99% of flatness (see panel (a)) can be conveniently replaced by a simulation with 10 walkers at 99% *fp* (panel (c)) or 100 walkers at 95% *fp* (panel (d)), since both require almost an order of magnitude less Monte Carlo steps. This is due to the averaging over each walker density result performed at the end of every Wang-Landau

iteration. Thus, after the parallelization into energy windows, it would be a good strategy to implement an additional parallelization by distributing different walkers onto different processors.

Table 3: Test of the performance of multiple walkers for the water molecule obtained using paradensum code. The exact DOS calculated with the doloop code has been considered as the reference to compute the Mean Relative Error MRE_j, according to Equation 12 in the text, where j identifies a specific run of the paradensum code which is initiated with a certain random number seed for the Monte Carlo procedure. For the other simulations, which are characterized by the number of walkers employed (Walkers) and the required flatness percentage (*fp*), the Table reports the average Mean Relative Error ($\overline{\mathrm{MRE}}$) and the σ calculated over 10 independent runs . The average Steps To Flatness (ave-STF) is obtained by averaging the total number of Monte Carlo steps needed to reach the convergence in each simulation over the 10 independent runs.

Panel (a)

Walkers	*fp*(%)	$\overline{MRE}$	σ	ave-STF
1	95	0.87	0.42	7.71×10^{8}
1	99	0.26	0.11	7.74×10^{9}
1	99.9	0.20	0.06	2.92×10^{11}
1	99.99	0.18	0.05	9.01×10^{11}

Panel (b)

Walkers	*fp*(%)	$\overline{MRE}$	σ	ave-STF
10	80	1.38	0.88	-
100	80	0.83	0.30	-
1000	80	0.39	0.07	5.92×10^{10}
10000	80	0.42	0.03	5.90×10^{11}

Panel (c)

Walkers	*fp*(%)	$\overline{MRE}$	σ	ave-STF
10	85	0.84	0.53	-
100	85	0.41	0.29	-
1000	85	0.29	0.07	9.64×10^{10}

Panel (d)

Walkers	*fp*(%)	$\overline{MRE}$	σ	ave-STF
10	90	0.63	0.30	-
100	90	0.21	0.05	1.92×10^{10}
1000	90	0.14	0.02	1.89×10^{11}

Panel (e)

Walkers	*fp*(%)	$\overline{MRE}$	σ	ave-STF
10	95	0.35	0.15	-
100	95	0.14	0.04	5.80×10^{10}
1000	95	0.13	0.02	5.78×10^{11}

Panel (f)

Walkers	*fp*(%)	$\overline{MRE}$	σ	ave-STF
10	99	0.14	0.03	5.47×10^{10}
100	99	0.10	0.01	5.25×10^{11}

Table 4: Test of the performance of multiple walkers for the calculation of the DOS of the TS of Cl + CH_4 reaction obtained using parsctst code. The results of the simulation with 100 walkers in each energy window and 99% of flatness (*fp*) has been considered as the reference to compute the Mean Relative Error MRE_j according to Equation 12 in the text. The index j identifies a specific run of the parsctst code which is initiated with a certain random number seed for the Monte Carlo procedure. The Table reports the average Mean Relative Error ($\overline{\text{MRE}}$) and the σ calculated over 10 independent runs for the other simulations which are characterized by the number of walkers employed (Walkers) and the required *fp*. The average Steps To Flatness (ave-STF) is obtained by averaging the total number of Monte Carlo steps needed to reach the convergence in each simulation over the 10 independent runs.

Panel (a)

Walkers	*fp*(%)	$\overline{MRE}$	σ	ave-STF
1	95	1.06	0.80	-
1	99	0.42	0.21	1.37×10^{10}
1	99.9	0.28	0.21	1.56×10^{11}
1	99.99	0.27	0.18	7.40×10^{11}

Panel (b)

Walkers	*fp*(%)	$\overline{MRE}$	σ	ave-STF
10	90	0.90	0.42	2.96×10^{9}
100	90	0.30	0.22	2.87×10^{10}
1000	90	0.22	0.09	2.86×10^{11}

Panel (c)

Walkers	*fp*(%)	$\overline{MRE}$	σ	ave-STF
10	95	0.36	0.12	9.20×10^{9}
100	95	0.18	0.07	8.91×10^{10}

Panel (d)

Walkers	*fp*(%)	$\overline{MRE}$	σ	ave-STF
10	99	0.13	0.07	9.00×10^{10}
100	99	0.00		8.46×10^{11}

4 Parallel Implementation Accuracy Check

Before applying our new implementation to a high dimensional reactive system, we check its reliability on the Cl + CH_4 reaction. For this purpose, we test the parallel codes against the serial ones, which are included in the MultiWell program suite[54] and are known to yield very accurate results with respect to experimental findings.[66,67] In both cases we start from the same input data. More specifically, the DOS for the CH_4 reactant and the transition state are based on harmonic vibrational frequencies calculated at the CCSD(T)/aug-cc-pVTZ level of theory. As for the $x_{j,j'}$ anharmonicity coefficients, the aug-cc-pVDZ basis set is employed for methane while aug-cc-pVTZ for the transition state.[66] We run the paradensum and parscts parallel codes on one side, and the serial bdens code for the reactants partition function and sctst code for the transition state on the other. To test the two approaches at the best of their capabilities, we employ 99% fp and 100 walkers in a run with 20 windows in the parallel implementation and set the highest allowed number of Monte Carlo sweeps (10^9) in the serial codes.

Figure 4 shows the final rate constant obtained with the two approaches. In the bottom panel, the temperature dependence of the rate constant computed with our parallel implementation is in close agreement with the one obtained with the MultiWell serial codes. This agreement is confirmed in a very wide range of temperatures as illustrated in the inset graph. To better assess any discrepancies between the two results, we report the percentage difference (% Diff.) in the upper panel. It is defined as $[k_{par}(T) - k_{ser}(T)] \times 100/k_{ser}(T)$, where $k_{par}(T)$ is the rate constant obtained with the parallel implementation, and $k_{ser}(T)$ is the one obtained with the serial codes. The deviation between the two results is always less than 1.5%. Moreover, it decreases and stabilizes below 0.5% at lower temperatures. We think the larger deviation in the high temperature regime is due to a slightly different counting of high energy states in the two implementations. In fact, in that energy range, the vibrational density of states is huge and the counting could be less precise. Notwithstanding, the overall agreement between the two results is very good and we can consider our implementation

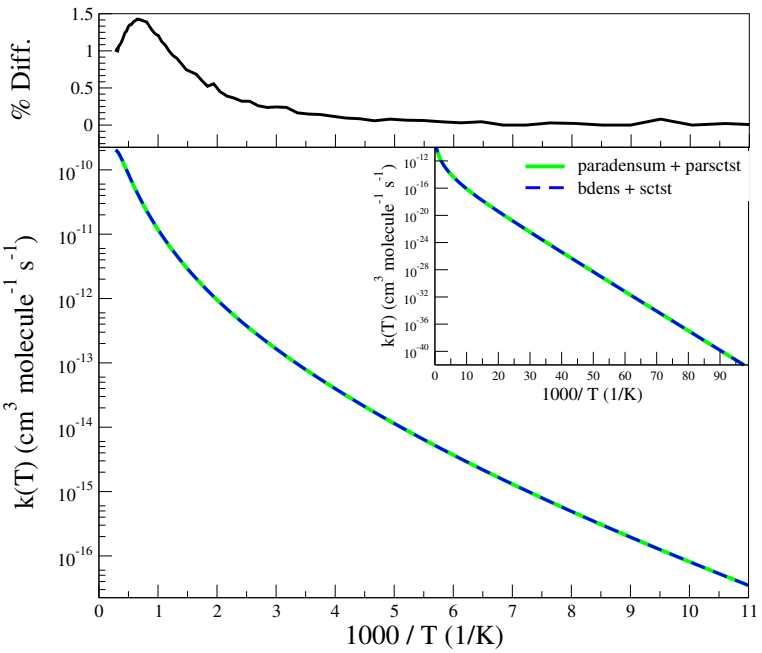

Figure 4: Comparison of the rate predicted by the parallel implementation (continuous green line) with the serial one (dashed blue line) contained in the MultiWell program suite. The bottom panel points out the agreement of the rate constant predicted by the two methods in the range between 90K and 350K, and the inset depicts the same result in a wider temperature range. In the top panel the percentage difference (% Diff.) between the two results is reported.

accurate and robust.

5 Application to a High Dimensional System

In this paragraph we apply the parallel implementation of SCTST to a high dimensional system. As a test case we choose the isomerization of the 2,4,6-tri-tert-butylphenyl to 3,5-ditert-butylneophyl, a 135 vibrational DOF system. This process is a proton transfer reaction and experimental measurements of the rate constants by Electron Paramagnetic Resonance spectroscopy (EPR) spotted the importance of a tunneling contribution. Specifically, Brunton et al. measured the rate constant for this reaction in the temperature range from 247K down to 113K,[68] and even at lower temperatures, down to 28K.[69] A significant non-Arrhenius behavior was observed by the emergence of a temperature-independent plateau in the thermal rate constant trend. In addition, experiments demonstrated that the solvent does not affect the reaction rate, since the rates of decay were identical when the reaction was conducted in different solvents such as propane, cyclopropane, isopentane, and toluene. For these reasons, we think that this example is the ideal test case for our parsctst implementation, because our approach does not account for the presence of the solvent. Moreover, Semiclassical Instanton (SCI) calculations are available for comparison.[70]

5.1 Ab Initio Calculations

To obtain reaction barrier heights, vibrational frequencies ω_j and the anharmonicity matrix elements $x_{jj'}$, we performed ab initio calculations. To begin with, we had to select a sufficiently accurate level of theory. For this system Coupled Cluster (CC) calculations are out of reach, therefore we relied on lower levels of theory. In the work by Meisner et al. DFT functionals were compared to the benchmark CC level of theory on a reduced dimensionality model for the reactive system.[70] They indicated that UB3LYP-D3/def2-TZVP is the best combination. In our Gaussian16 DFT calculations,[46] we adopt the model chemistry

UB3LYP/6-311G** + D3. For comparison, we performed MP2/6-311G** calculations using the NWChem suite of codes.[71]

To assess the choice of the basis set, we performed benchmark calculations on the Phenyl radical, the simplest Aryl radical. The reference geometry is depicted in Figure 5. For

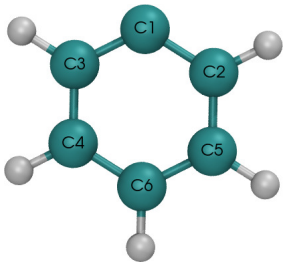

Figure 5: Reference geometry of the Phenyl radical for basis set assessment. See Table 5 for bond lengths and angles values.

this system CCSD(T)/cc-CVQZ calculations are available in the literature.[72] We therefore compared some structural parameters and $\langle S^2 \rangle$ to those calculated at the CC level of theory. The latter quantity has to be checked against its exact value $S(S+1)\hbar^2$ in this case, since the unrestricted wavefunction by definition is not an eigenfunction of S^2. These results are reported in Table 5. The best over-all accuracy is achieved with the 6-311G** basis set.

Table 5: Basis set benchmark calculations for UB3LYP + D3 calculations on Phenyl radical. The "Ref." column reports structural parameters from CCSD(T)/cc-CVQZ and S^2 exact value.[72] The reference geometry is sketched in Figure 5. Next columns report the percentage deviations of each parameter computed with a certain basis set from the reference values.

	Ref.	6-311G	6-311G**	cc-pVDZ	cc-pVTZ	cc-pVQZ
Bond length C1-C2(C3)	1.3733Å	-0.54	-0.09	-0.54	0.18	0.23
Angle C3-C1-C2	125.83°	0.29	-0.02	0.06	-0.12	-0.15
Angle C1-C3-C4(C5)	116.62°	-0.18	0.03	0.02	0.09	0.10
$<S^2>$	0.75	-1.11	-1.09	-1.09	-0.92	-0.92

We have optimized the structures of the reactant (R), product (P) and the transition state (TS) with UB3LYP/6-311G** + D3, with and without Polarizable Continuum Model (PCM) of toluene solvent,[73] and with UMP2/6-311G** model chemistry too. We found

structures very similar to each other, and we have represented the UB3LYP/6-311G** + D3 structures in Figure 6. These geometries show that along the minimum energy path one of

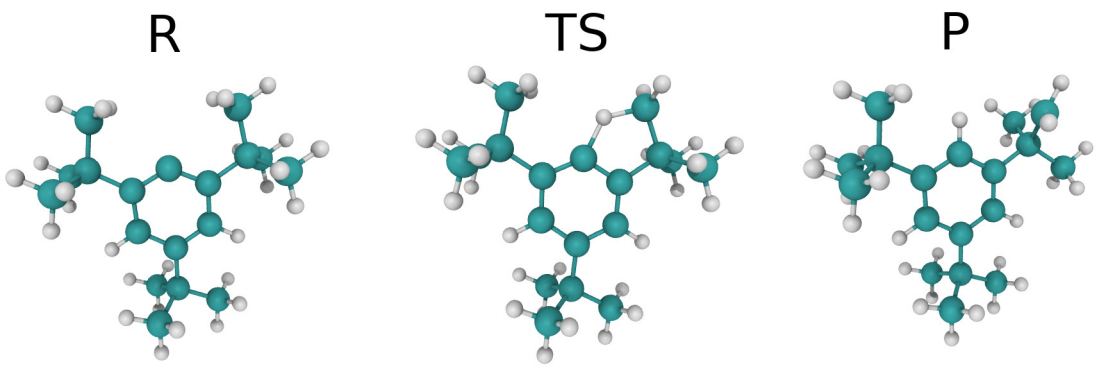

Figure 6: Structures of the stationary points on the PES for the isomerization of the 2,4,6-tri-tert-butylphenyl to 3,5-di-tert-butylneophyl at UB3LYP/6-311G** + D3 level of theory. R is the reactant structure, P the products one, while TS is the geometry associated to the transition state.

the methyl groups next to the carbon radical in the reactant structure R rotates around its C-C bond and donates the proton that finally saturates the phenyl ring (see the transition state structure TS). After that, the tert-Butyl which contains the donor methyl group rotates around the C-C bond with the ring and settles down in the P structure. This is consistent with what was found in previous studies on the same system.[70] Table 6 reports the forward barrier (E_f) and backwards barrier (E_r) corrected by the harmonic Zero Point Energies (ZPE) at three different levels of theory. UB3LYP results are in close agreement with the values already provided in literature. It is interesting that adding the PCM of toluene, the barrier height is affected only by the 0.06% in the forward direction and by the 0.08% in the reverse one. This is in agreement with the already mentioned experimental observations that the solvent is not relevant for the kinetics of this reaction.[68,69] The barrier computed at the level of UMP2 is higher in energy than the one predicted by DFT, both in the forward and in the backward directions.

Table 6: Forward (E_f) and backward (E_r) reaction barriers for the isomerization of the 2,4,6-tri-tert-butylphenyl to 3,5-di-tert-butylneophyl computed with different levels of theory. The PCM in the third line is used to account for the presence of toluene solvent. UB3LYP-D3/def2-TZVP are taken from reference[70].

	E_f (kJ/mol)	E_r (kJ/mol)
UB3LYP-D3/def2-TZVP	64.00	99.8
UB3LYP/6-311G** + D3	63.83	97.99
UB3LYP/6-311G** + D3 + PCM	63.87	98.07
UMP2/6-311G**	69.27	130.10

5.2 Rate Constants

We computed normal mode frequencies and the anharmonic $x_{jj'}$ matrix elements for structure R and the TS geometry only at the DFT level of theory, because the VPT2 computation at MP2 level was impractical for this high dimensional system. Our goal in this work is to demonstrate the applicability of our parallel implementation to high dimensional systems rather than to get the highly accurate rate constant results, that can be achieved only with very high level electronic structure calculations, as discussed elsewhere.[48] The plot displayed in Figure 7 summarizes rate constant calculations conducted with different parameters and compares with other methods. All data presented were obtained with the Wang-Landau flatness criterion fixed at 95% and the parallelization was done with twenty windows with one walker each. The energy bin width was set to 5 cm^{-1}. As expected, classical Transition State Theory (TST) employing the UB3LYP/6-311G** + D3 barrier and normal mode frequencies appears as a straight line on the Arrhenius plot, showing that no quantum or anharmonic effects are reproduced. When we employ the SCTST rate formulation without accounting for anharmonicity, i.e. setting all $x_{jj'}$ matrix elements to zero, a curve that merges with TST at high temperatures is found (see the dot-dashed line in Figure 7). This approach heavily overestimates tunneling at low temperatures. Instead, when anharmonic couplings of all DOFs are included, the rate obtained at the same level of theory is significantly more accurate, as shown by the blue line in Figure 7. However, at low temperature, theory is

still off the mark. We believe that this large deviation is mainly due to the level of theory, i.e. DFT, which gives barrier height values that are somewhat low, although we expect that it is accurate enough for harmonic and anharmonic constants. Thus, we have arbitrarily raised the barrier height by 10kJ/mol and obtained the dotted line in Figure 7. Remarkably these results are in excellent agreement with the experimental values and with the SCI calculations,[70] which were performed with the same functional, but a slightly different basis set. This suggests further studies should be aimed at comparing the SCI and the SCTST methods for better assessing the physics behind each approximation. In order to recover more accurate results, fully ab initio and without any ad hoc adjustment, we estimate the barrier height using the MP2 level of theory. The results are reported as a continuous red line in Figure 7 and they are significantly more accurate than the DFT results, but still differ from the experiments. These results demonstrate the dramatic importance of vibrational coupling and anharmonicity, as well as that of tunneling in high-dimensional systems.

6 Summary and Conclusions

In this paper we have presented a parallel implementation of the SCTST method that makes it possible to obtain non empirical tunneling corrections in anharmonic rate constant calculations for high dimensional systems, with an affordable computational overhead. We performed the parallelization of part of the MultiWell suite of codes, which has already been presented in the literature,[54] and obtained a highly efficient code, as demonstrated by the almost ideal speedup of the high dimensional system simulations.

To prove the applicability of the code to high dimensional reactive system, we applied it to the isomerization reaction of the 2,4,6-tri-tert-butylphenyl to 3,5-di-tert-butylneophyl, which consists of 135 vibrational DOFs. This process is known to be characterized by quantum tunneling at low temperature. We obtained a satisfactory qualitative agreement with the experimental data, by employing the DFT level of electronic theory. However, we showed

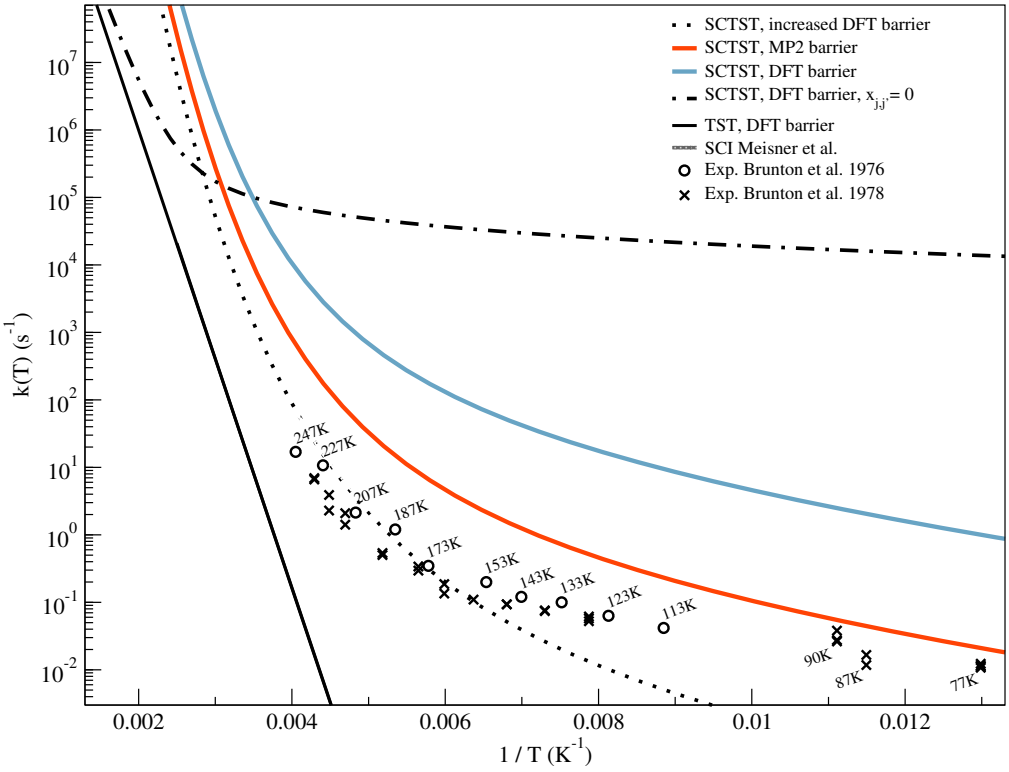

Figure 7: Plot of the rate constant as a function of the inverse of temperature for the isomerization of the 2,4,6-tri-tert-butylphenyl to 3,5-di-tert-butylneophyl. Black continuous line is the TST result computed with UB3LYP/6-311G** + D3 barrier. Dots and crosses are two experimental data sets form Brunton et al.[68,69] Dot-dashed line is the SCTST harmonic result computed with UB3LYP/6-311G** + D3 barrier. Blue line is SCTST result at UB3LYP/6-311G** + D3 level of theory, while red line is SCTST result with anharmonic couplings and frequencies from UB3LYP/6-311G** + D3, but barrier from UMP2/6-311G**. Grey line are the SCI result from the literature.[70] The black dotted line stands for SCTST result based on UB3LYP/6-311G** + D3 if the reaction barrier is increased by 10 kJ/mol.

that our rate estimates can be consistently improved if the electronic structure calculations were done at a higher level of theory. For instance, when we replaced the height of the DFT barrier with the one computed at MP2 level, results were clearly improved.

The VPT2/SCTST approach has been proved to provide really accurate rates if the electronic structure calculations are performed at Coupled Cluster level[48]. With the present SCTST parallelization, which significantly reduces the DOS and rate calculation computational effort, the preponderant computational effort for rate estimates is left to the ab initio quantum chemistry part.

The parsctst code will be distributed as an open source code in the next release of the MultiWell program suite under the GNU General Public License. A further development would be to include our parallel strategy into the MultiWell bdens code which computes the density of states exactly at low energies (replacing the doloop code) and uses the Wang-Landau approach at higher energy.

Acknowledgments

We thank Università degli Studi di Milano for computational time at CINECA (Italian Supercomputing Center). We warmly thank Professor J. R. Barker for useful discussions and carefully reading the manuscript.

References

(1) Miller, W. H. *Direct* and *correct* calculation of canonical and microcanonical rate constants for chemical reactions. *J. Phys. Chem. A* **1998**, *102*, 793–806.

(2) Miller, W. H. Coupled equations and the minimum principle for collisions of an atom and a diatomic molecule, including rearrangements. *J. Chem. Phys.* **1969**, *50*, 407–418.

(3) Tromp, J. W.; Miller, W. H. The reactive flux correlation function for collinear reactions $H + H_2$, $Cl + HCl$ and $F + H_2$. *Faraday Discuss. Chem. Soc.* **1987**, *84*, 441–453.

(4) Wang, H.; Thompson, W. H.; Miller, W. H. Thermal rate constant calculation using flux–flux autocorrelation functions: Application to $Cl + H_2 \rightarrow HCl + H$ reaction. *J. Chem. Phys.* **1997**, *107*, 7194–7201.

(5) Thompson, W. H.; Miller, W. H. On the *direct* calculation of thermal rate constants. II. The flux-flux autocorrelation function with absorbing potentials, with application to the $O + HCl \rightarrow OH + Cl$ reaction. *J. Chem. Phys.* **1997**, *106*, 142–150.

(6) Park, T. J.; Light, J. Quantum flux operators and thermal rate constant: Collinear $H + H_2$. *J. Chem. Phys.* **1988**, *88*, 4897–4912.

(7) Day, P. N.; Truhlar, D. G. Calculation of thermal rate coefficients from the quantum flux autocorrelation function: Converged results and variational quantum transition state theory for $O + HD \leftrightarrow OD + H$ and $O + HD \leftrightarrow OH + D$. *J. Chem. Phys.* **1991**, *95*, 5097–5112.

(8) Nyman, G. Computational methods of quantum reaction dynamics. *Int. J. Quantum Chem.* **2014**, *114*, 1183–1198.

(9) Zhang, D. H.; Guo, H. Recent advances in quantum dynamics of bimolecular reactions. *Annu. Rev. Phys. Chem.* **2016**, *67*, 135–158.

(10) Matzkies, F.; Manthe, U. Accurate quantum calculations of thermal rate constants employing MCTDH: $H_2 + OH \rightarrow H + H_2O$ and $D_2 + OH \rightarrow D + DOH$. *J. Chem. Phys.* **1998**, *108*, 4828–4836.

(11) Manthe, U.; Matzkies, F. Quantum calculations of thermal rate constants and reaction probabilities: $H_2 + CN \rightarrow H + HCN$. *Chem. Phys. Lett.* **1998**, *282*, 442–449.

(12) Welsch, R.; Manthe, U. Full-dimensional and reduced-dimensional calculations of initial state-selected reaction probabilities studying the $H + CH_4 \rightarrow H_2 + CH_3$ reaction on a neural network PES. *The Journal of chemical physics* **2015**, *142*, 064309.

(13) Welsch, R. Low-Temperature Thermal Rate Constants for the Water Formation Reaction $H_2 + OH$ from Rigorous Quantum Dynamics Calculations. *Angew. Chem.* **2018**, *130*, 13334–13337.

(14) Sun, P.; Zhang, Z.; Chen, J.; Liu, S.; Zhang, D. H. Well converged quantum rate constants for the $H_2 + OH \rightarrow H_2O + H$ reaction via transition state wave packet. *J. Chem. Phys.* **2018**, *149*, 064303.

(15) Ellerbrock, R.; Manthe, U. Full-dimensional quantum dynamics calculations for $H + CHD_3 \rightarrow H_2 + CD_3$: The effect of multiple vibrational excitations. *J. Chem. Phys.* **2018**, *148*, 224303.

(16) Sumathi, R.; Green Jr., W. H. A priori rate constants for kinetic modeling. *Theor. Chem. Acc.* **2002**, *108*, 187–213.

(17) Eyring, H. The activated complex in chemical reactions. *J. Chem. Phys.* **1935**, *3*, 107–115.

(18) Wigner, E. Calculation of the rate of elementary association reactions. *J. Chem. Phys.* **1937**, *5*, 720–725.

(19) Truhlar, D. G.; Garrett, B. C. Variational transition-state theory. *Acc. Chem. Res.* **1980**, *13*, 440–448.

(20) Bao, J. L.; Sripa, P.; Truhlar, D. G. Path-dependent variational effects and multidimensional tunneling in multi-path variational transition state theory: rate constants calculated for the reactions of HO2 with tert-butanol by including all 46 paths for ab-

straction at C and all six paths for abstraction at O. *Phys. Chem. Chem. Phys.* **2016**, *18*, 1032–1041.

(21) Meisner, J.; Kästner, J. Atom tunneling in chemistry. *Angew. Chem. Int. Ed. Engl.* **2016**, *55*, 5400–5413.

(22) Craig, I. R.; Manolopoulos, D. E. Quantum statistics and classical mechanics: Real time correlation functions from ring polymer molecular dynamics. *J. Chem. Phys.* **2004**, *121*, 3368–3373.

(23) Hele, T. J.; Althorpe, S. C. Derivation of a true $(t \to 0 + 1)$ quantum transition-state theory. I. Uniqueness and equivalence to ring-polymer molecular dynamics transition-state-theory. *J. Chem. Phys.* **2013**, *138*, 084108.

(24) Richardson, J. O. Perspective: Ring-polymer instanton theory. *J. Chem. Phys.* **2018**, *148*, 200901.

(25) Voth, G. A.; Chandler, D.; Miller, W. H. Rigorous formulation of quantum transition state theory and its dynamical corrections. *J. Chme. Phys.* **1989**, *91*, 7749–7760.

(26) Jang, S.; Voth, G. A. Non-uniqueness of quantum transition state theory and general dividing surfaces in the path integral space. *J. Chem. Phys.* **2017**, *146*, 174106.

(27) Miller, W. H.; Zhao, Y.; Ceotto, M.; Yang, S. Quantum instanton approximation for thermal rate constants of chemical reactions. *J. Chem. Phys.* **2003**, *119*, 1329–1342.

(28) Ceotto, M.; Miller, W. H. Test of the quantum instanton approximation for thermal rate constants for some collinear reactions. *J. Chem. Phys.* **2004**, *120*, 6356–6362.

(29) Ceotto, M.; Yang, S.; Miller, W. H. Quantum reaction rate from higher derivatives of the thermal flux-flux autocorrelation function at time zero. *J. Chem. Phys.* **2005**, *122*, 044109.

(30) Aieta, C.; Ceotto, M. A quantum method for thermal rate constant calculations from stationary phase approximation of the thermal flux-flux correlation function integral. *The Journal of Chemical Physics* **2017**, *146*, 214115.

(31) Pollak, E.; Liao, J.-L. A new quantum transition state theory. *J. Chem. Phys.* **1998**, *108*, 2733–2743.

(32) Liao, J.-L.; Pollak, E. Quantum Transition State Theory for the Collinear $H + H_2$ Reaction. *J. Phys. Chem. A* **2000**, *104*, 1799–1803.

(33) Miller, W. H. Importance of nonseparability in quantum mechanical transition-state theory. *Acc. Chem. Res.* **1976**, *9*, 306–312.

(34) Child, M. S. *Semiclassical mechanics with molecular applications*; Oxford University Press, USA, 2014.

(35) Schatz, G. C.; Ratner, M. A. *Quantum mechanics in chemistry*; Courier Corporation, 1993.

(36) Miller, W. H. Semiclassical limit of quantum mechanical transition state theory for nonseparable systems. *J. Chem. Phys.* **1975**, *62*, 1899–1906.

(37) Affleck, I. Quantum-statistical metastability. *Phys. Rev. Lett.* **1981**, *46*, 388.

(38) Mills, G.; Schenter, G.; Makarov, D.; Jónsson, H. Generalized path integral based quantum transition state theory. *Chem. Phys. Lett.* **1997**, *278*, 91 – 96.

(39) Kryvohuz, M. Semiclassical instanton approach to calculation of reaction rate constants in multidimensional chemical systems. *J. Chem. Phys.* **2011**, *134*, 114103.

(40) Kryvohuz, M. Calculation of chemical reaction rate constants using on-the-fly high level electronic structure computations with account of multidimensional tunneling. *J. Chem. Phys.* **2012**, *137*, 234304.

(41) Miller, W. H.; Schwartz, S. D.; Tromp, J. W. Quantum mechanical rate constants for bimolecular reactions. *J. Chem. Phys.* **1983**, *79*, 4889–4898.

(42) Ceotto, M. Vibration-assisted tunneling: a semiclassical instanton approach. *Mol. Phys.* **2012**, *110*, 547–559.

(43) Beyer, A. N.; Richardson, J. O.; Knowles, P. J.; Rommel, J.; Althorpe, S. C. Quantum Tunneling Rates of Gas-Phase Reactions from On-the-Fly Instanton Calculations. *J. Phys. Chem. Lett.* **2016**, *7*, 4374–4379.

(44) Richardson, J. O. Derivation of instanton rate theory from first principles. *J. Chem. Phys.* **2016**, *144*, 114106.

(45) Hernandez, R.; Miller, W. H. Semiclassical transition state theory. A new perspective. *Chem. Phys. Lett.* **1993**, *214*, 129–136.

(46) Frisch, M. J.; Trucks, G. W.; Schlegel, H. B.; Scuseria, G. E.; Robb, M. A.; Cheeseman, J. R.; Scalmani, G.; Barone, V.; Petersson, G. A.; Nakatsuji, H.; Li, X.; Caricato, M.; Marenich, A. V.; Bloino, J.; Janesko, B. G.; Gomperts, R.; Mennucci, B.; Hratchian, H. P.; Ortiz, J. V.; Izmaylov, A. F.; Sonnenberg, J. L.; Williams-Young, D.; Ding, F.; Lipparini, F.; Egidi, F.; Goings, J.; Peng, B.; Petrone, A.; Henderson, T.; Ranasinghe, D.; Zakrzewski, V. G.; Gao, J.; Rega, N.; Zheng, G.; Liang, W.; Hada, M.; Ehara, M.; Toyota, K.; Fukuda, R.; Hasegawa, J.; Ishida, M.; Nakajima, T.; Honda, Y.; Kitao, O.; Nakai, H.; Vreven, T.; Throssell, K.; Montgomery, J. A., Jr.; Peralta, J. E.; Ogliaro, F.; Bearpark, M. J.; Heyd, J. J.; Brothers, E. N.; Kudin, K. N.; Staroverov, V. N.; Keith, T. A.; Kobayashi, R.; Normand, J.; Raghavachari, K.; Rendell, A. P.; Burant, J. C.; Iyengar, S. S.; Tomasi, J.; Cossi, M.; Millam, J. M.; Klene, M.; Adamo, C.; Cammi, R.; Ochterski, J. W.; Martin, R. L.; Morokuma, K.; Farkas, O.; Foresman, J. B.; Fox, D. J. Gaussian16 Revision A.03. 2016; Gaussian Inc. Wallingford CT.

(47) Stanton, J. F.; Gauss, J.; Cheng, L.; Harding, M. E.; Matthews, D. A.; Szalay, P. G. CFOUR, Coupled-Cluster techniques for Computational Chemistry, a quantum-chemical program package. With contributions from A.A. Auer, R.J. Bartlett, U. Benedikt, C. Berger, D.E. Bernholdt, Y.J. Bomble, O. Christiansen, F. Engel, R. Faber, M. Heckert, O. Heun, M. Hilgenberg, C. Huber, T.-C. Jagau, D. Jonsson, J. Jusélius, T. Kirsch, K. Klein, W.J. Lauderdale, F. Lipparini, T. Metzroth, L.A. Mück, D.P. O'Neill, D.R. Price, E. Prochnow, C. Puzzarini, K. Ruud, F. Schiffmann, W. Schwalbach, C. Simmons, S. Stopkowicz, A. Tajti, J. Vázquez, F. Wang, J.D. Watts and the integral packages MOLECULE (J. Almlöf and P.R. Taylor), PROPS (P.R. Taylor), ABACUS (T. Helgaker, H.J. Aa. Jensen, P. Jørgensen, and J. Olsen), and ECP routines by A. V. Mitin and C. van Wüllen. For the current version, see http://www.cfour.de.

(48) Nguyen, T. L.; Barker, J. R.; Stanton, J. F. Atmospheric Reaction Rate Constants and Kinetic Isotope Effects Computed Using the HEAT Protocol and Semi-Classical Transition State Theory. *Adv. Atmos. Chem.* **2017**, 403–492.

(49) Peters, B.; Bell, A. T.; Chakraborty, A. Rate constants from the reaction path Hamiltonian. II. Nonseparable semiclassical transition state theory. *J. Chem. Phys.* **2004**, *121*, 4461–4466.

(50) Greene, S. M.; Shan, X.; Clary, D. C. Rate constants of chemical reactions from semiclassical transition state theory in full and one dimension. *J. Chem. Phys.* **2016**, *144*, 244116.

(51) Greene, S. M.; Shan, X.; Clary, D. C. Reduced-Dimensionality Semiclassical Transition State Theory: Application to Hydrogen Atom Abstraction and Exchange Reactions of Hydrocarbons. *J. Phys. Chem. A* **2015**, *119*, 12015–12027.

(52) Greene, S. M.; Shan, X.; Clary, D. C. An investigation of one- versus two-dimensional

semiclassical transition state theory for H atom abstraction and exchange reactions. *J. Chem. Phys.* **2016**, *144*.

(53) Skouteris, D.; Calderini, D.; Barone, V. Methods for calculating partition functions of molecules involving large amplitude and/or anharmonic motions. *J. Chem. Theory Comput.* **2016**, *12*, 1011–1018.

(54) MultiWell-2017 Software Suite. J.R. Barker, T.L. Nguyen, J.F. Stanton, C. Aieta, M. Ceotto, F. Gabas, T.J.D. Kumar, C.G.L. Li, L.L. Lohr, A. Maranzana, N.F. Ortiz, J.M. Preses, J.M. Simmie, J.A. Sonk, and P.J. Stimac, University of Michigan, Ann Arbor, Michigan, USA, 2016. http://clasp-research.engin.umich.edu/multiwell/.

(55) Barker, J. R. Multiple-Well, multiple-path unimolecular reaction systems. I. MultiWell computer program suite. *Int. J. Chem. Kinet.* **2001**, *33*, 232–245.

(56) Barker, J. R. Energy transfer in master equation simulations: A new approach. *Int. J. Chem. Kinet.* **2009**, *41*, 748–763.

(57) Wang, F.; Landau, D. Determining the density of states for classical statistical models: A random walk algorithm to produce a flat histogram. *Phys. Rev. E* **2001**, *64*, 056101.

(58) Nguyen, T. L.; Barker, J. R. Sums and densities of fully coupled anharmonic vibrational states: A comparison of three practical methods. *J. Phys. Chem. A* **2010**, *114*, 3718–3730.

(59) Nguyen, T. L.; Stanton, J. F.; Barker, J. R. A practical implementation of semi-classical transition state theory for polyatomics. *Chem. Phys. Lett.* **2010**, *499*, 9–15.

(60) Aieta, C.; Gabas, F.; Ceotto, M. An efficient computational approach for the calculation of the vibrational density of states. *J. Phys. Chem. A* **2016**, *120*, 4853–4862.

(61) Miller, W. H. Semi-classical theory for non-separable systems: Construction of "good"

action-angle variables for reaction rate constants. *Faraday Discuss. Chem. Soc.* **1977**, *62*, 40–46.

(62) Miller, W. H.; Hernandez, R.; Handy, N. C.; Jayatilaka, D.; Willetts, A. Ab initio calculation of anharmonic constants for a transition state, with application to semiclassical transition state tunneling probabilities. *Chem. Phys. Lett.* **1990**, *172*, 62–68.

(63) Stanton, J. F. Semiclassical Transition-State Theory Based on Fourth-Order Vibrational Perturbation Theory: The Symmetrical Eckart Barrier. *J. Phys. Chem. Lett.* **2016**, *7*, 2708–2713.

(64) Beyer, T.; Swinehart, D. Algorithm 448: number of multiply-restricted partitions. *Commun. ACM* **1973**, *16*, 379.

(65) Vogel, T.; Li, Y. W.; Wüst, T.; Landau, D. P. Generic, hierarchical framework for massively parallel Wang-Landau sampling. *Physical review letters* **2013**, *110*, 210603.

(66) Barker, J. R.; Nguyen, T. L.; Stanton, J. F. Kinetic Isotope Effects for Cl + CH4 â HCl + CH3 Calculated Using ab Initio Semiclassical Transition State Theory. *The Journal of Physical Chemistry A* **2012**, *116*, 6408–6419, PMID: 22295940.

(67) Nguyen, T. L.; Barker, J. R.; Stanton, J. F. *Advances in Atmospheric Chemistry*; World Scientific, 2017; pp 403–492.

(68) Brunton, G.; Griller, D.; Barclay, L.; Ingold, K. Kinetic applications of electron paramagnetic resonance spectroscopy. 26. Quantum-mechanical tunneling in the isomerization of sterically hindered aryl radicals. *J. Am. Chem. Soc.* **1976**, *98*, 6803–6811.

(69) Brunton, G.; Gray, J. A.; Griller, D.; Barclay, L.; Ingold, K. Kinetic applications of electron paramagnetic resonance spectroscopy. 32. Further studies of quantum-mechanical tunneling in the isomerization of sterically hindered aryl radicals. *J. Am. Chem. Soc.* **1978**, *100*, 4197–4200.

(70) Meisner, J.; Markmeyer, M. N.; Bohner, M. U.; Kästner, J. Comparison of classical reaction paths and tunneling paths studied with the semiclassical instanton theory. *Phys. Chem. Chem. Phys.* **2017**, *19*, 23085–23094.

(71) Valiev, M.; Bylaska, E.; Govind, N.; Kowalski, K.; Straatsma, T.; Dam, H. V.; Wang, D.; Nieplocha, J.; Apra, E.; Windus, T.; de Jong, W. NWChem: A comprehensive and scalable open-source solution for large scale molecular simulations. *Comput. Phys. Commun.* **2010**, *181*, 1477 – 1489.

(72) Martinez Jr, O.; Crabtree, K. N.; Gottlieb, C. A.; Stanton, J. F.; McCarthy, M. C. An accurate molecular structure of phenyl, the simplest aryl radical. *Angew. Chem.* **2015**, *127*, 1828–1831.

(73) Mennucci, B. Polarizable continuum model. *Wiley Interdiscip. Rev.: Comput. Mol. Sci.* **2012**, *2*, 386–404.

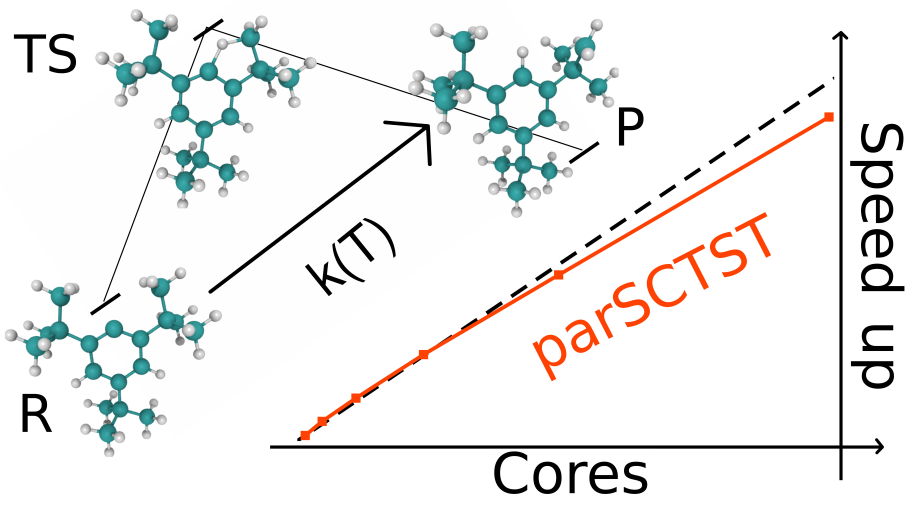
TS
P
R
k(T)
parSCTST
Speed up
Cores